Macromolecular Chemistry and Physics
www.mcp-journal.de

Influence of Post-Synthesis Heat Treatments on the Molecular Structure and Thermal Stability of Phosphatized Starch

*Florian Rothenhäusler, Felix Ludik, Rika Schneider, Felix Bretschneider, Beate Bojer, Helen Grüninger, Andreas Greiner, and Holger Ruckdaeschel**

The threat of fires necessitates effective flame retardants (FR) to safeguard human life and property. In response to the demand for sustainable options, bio-based FR have emerged, with phosphatized starch (PS) standing out as a promising candidate. This study explores the influence of post-synthesis heat treatments on the molecular structure of PS to enhance its thermal stability for processing in polymeric matrix materials. The molecular structure of the flame-retardant PS is characterized via solid state and solution nuclear magnetic resonance spectroscopy, Fourier-transform infrared spectroscopy, and differential scanning calorimetry. Through a comprehensive analysis of results from thermo-gravimetric analysis, thermo-gravimetric Fourier-transform infrared spectroscopy, and elemental analysis, the thermal stability and thermal decomposition mechanisms of PS are investigated. The post-synthesis heat treatment leads to the decomposition of residual urea and carbamate groups, as well as to the formation of ammonium polyphosphates. By employing thermal modification, the thermal stability and phosphorus-content are enhanced.

1. Introduction

The threat of fires poses a significant hazard to both human life and property, underscoring the vital importance of effective flame retardants (FR).[1–3] FR are chemical additives used to reduce the flammability of various materials, thereby mitigating the risks associated with fires.[4] However, the conventional use of halogenated FR, once widely embraced for their effectiveness, are increasingly facing scrutiny and even bans in several parts of the world due to their persistence in the environment, potential toxicity, and the formation of hazardous by-products when exposed to fire.[5–7] This necessitates the search for more environmentally friendly and health-conscious alternatives to meet the ever-increasing demand for fire-safe materials. Among the potential alternatives, phosphorus-based FR have emerged as a promising solution to address these concerns.[8]

Phosphorus-based FR offer several advantages over their halogenated counterparts. They are recognized for their ability to efficiently inhibit combustion by promoting char formation, which serves as a protective, intumescent barrier, preventing the spread of flames.[9,10] Additionally, the radical chain reaction in the flame zone is interrupted by phosphorus-containing radicals that form as result of the combustion process.[9,11] Thereby, they produce significantly fewer toxic by-products when exposed to fire, making them a safer choice for fire safety applications.[12] Moreover, phosphorus-based FR exhibit a lower environmental impact and are increasingly being employed as an eco-friendly option.[13]

In light of the environmental and health concerns surrounding traditional FR, there has been a growing interest in developing bio-based, phosphorous FR, reducing the reliance on non-renewable raw materials and minimizing the carbon footprint.[14] As part of this sustainable approach, phosphatized starch (PS) has emerged as a compelling candidate among bio-based FR.[15,16] Starch, a natural polymer derived from plants, is abundant and readily available, making it an ideal feedstock for sustainable FR development.[17] PS is usually derived by mixing urea and phosphatizing-agents with starch and letting it react at temperatures at ≈135°C for several hours.[18] As a result, the hydroxyl groups of the anhydroglucose units (AGU) are transformed into a variety of different esters containing functional groups, such as phosphate, ammonium phosphates and carbamate groups, depending on the ratio of starch to the phosphatizing-agents and urea, and reaction temperature and time (see **Figure 1**).[18,19] PS, in particular, shows promise as a sustainable FR as it combines the inherent flame-retardant properties

F. Rothenhäusler, F. Ludik, H. Ruckdaeschel
Department of Polymer Engineering
University of Bayreuth
Universitätsstraße 30, 95447 Bayreuth, Germany
E-mail: holger.ruckdaeschel@uni-bayreuth.de
R. Schneider, F. Bretschneider, A. Greiner
Macromolecular Chemistry II
University of Bayreuth
Universitätsstraße 30, 95447 Bayreuth, Germany
B. Bojer, H. Grüninger
Inorganic Chemistry III
University of Bayreuth
Universitätsstraße 30, 95447 Bayreuth, Germany

DOI: 10.1002/macp.202400252

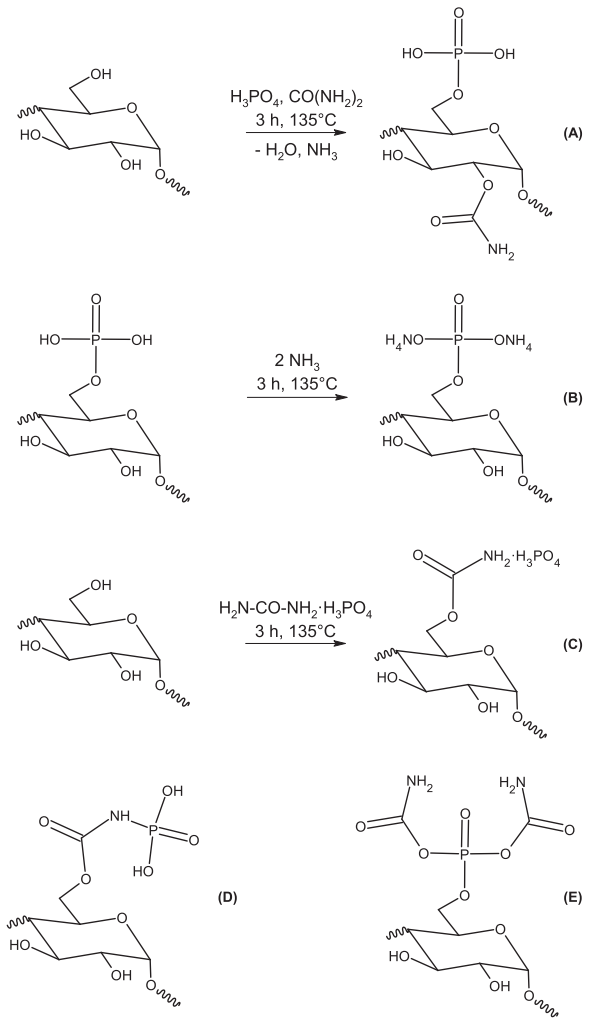

Figure 1. Functional groups resulting from the reaction of starch, urea and phosphoric acid according to Passauer et al.[19]: A) Starch phosphates carbamates, B) ammonium starch phosphate, C) starch carbamate phosphate with blocked amino group, D) starch phosphoric amide, and E) starch carbamoyl phosphate.

of phosphorus with the renewable and biodegradable nature of starch. By the presence of both nitrogen and phosphorus in PS the phosphorus-nitrogen synergism can be utilized.[20–22]

PS has already been used as an FR for wood fibers, expandable polystyrene foams, paper and cotton.[23–27] In dynamic thermogravimetric analysis (TGA) of the PS it was noted that mass loss occurred at ≈133°C as the result of urea decomposition.[28,29] Thereby, volatile ammonia and isocyanic acid are released as gases.[30] The isocyanic acid itself is hydrolyzed into carbon dioxide and ammonia.[31] Another concern is the decomposition of carbamate groups into ammonia and carbon dioxide.[25] Previous studies on the reactions in the starch–urea–phosphoric acid system proposed a series of condensation reactions that might lead to the release of ammonia.[32–34] The release of gases via decomposition or condensation reactions that occur in PS at elevated temperatures causes pores in the polymeric matrix material during processing. This phenomenon has yet to be addressed in literature to enable the application of PS as an FR for polymers whose processing takes place at elevated temperatures.

This paper explores the influence of post-synthesis heat treatments on the molecular structure of PS to enhance its thermal stability for processing in polymeric matrix materials. The molecular structure of the flame-retardant PS is characterized via solid state and solution nuclear magnetic resonance spectroscopy (NMR), Fourier-transform infrared spectroscopy (FTIR), and differential scanning calorimetry (DSC). Through a comprehensive analysis of results from thermo-gravimetric analysis (TGA), thermo-gravimetric Fourier-transform infrared spectroscopy (TGFTIR), and elemental analysis, the thermal stability and thermal decomposition mechanisms of PS are investigated.

2. Experimental Section

2.1. Materials

Wheat starch was sourced from VWR Chemicals (Radnor, PA, US). Urea (≥99.5 %) used was purchased from Carl Roth GmbH (Karlsruhe, Germany) and the phosphoric acid (85 %) from Fisher Scientific GmbH (Schwerte, Germany). All chemicals were used as received.

2.2. Synthesis

100 g of wheat starch (616.8 mmol; 1 eq) were thoroughly mixed with 222.3 g of urea (3.7 mol; 6 eq). Subsequently, 83.2 mL of phosphoric acid (1.23 mol; 2 eq) were added to the solid mixture and blended firmly to form a paste-like mass. The resulting mixture was placed in a vacuum oven at 135°C and 60mbar for 2 h to react, during which it exhibited vigorous foaming.

After the reaction period, the mass was cooled to room temperature, and water was added, causing the solid to swell. Following this, methanol was added until the solid precipitated completely. The solution was decanted, and the solid was washed twice more with aqueous methanol (80 % by volume). Subsequently, the solid was stirred for 30 min in pure methanol, then filtered off, and dried overnight at 50°C in a vacuum oven. The resulting PS was obtained as an almost white powder. The synthesis procedure followed the methodology described by Heinze et al.[18]

However, the resulting PS proved unsuitable for polymer processing methods requiring temperatures as low as 100°C, due to the presence of thermally unstable carbamate and ammonium phosphate groups, as well as residual urea. To address this, a heat treatment was conducted using an IKA RV 10 rotary evaporator from IKA Werke GmbH & Co. KG (Staufen im Breisgau, Germany). The PS was placed in a 2 L round-bottom flask and heated in an oil bath at 160°C for 3 h, with the rotary speed set to 20 min^{-1} and a vacuum pressure of 150mbar applied (temperature monitored with an analog thermometer with a precision of ±0.1°C). It is essential to note that the 160°C in the oil bath does not directly translate to 160°C in the round-bottom flask, a critical consideration for avoiding excessive glycosidic bond cleavage (GBC) during heat treatment, as discussed in the results.

For analysis of thermal decomposition processes, samples were extracted every 30 min up to 180 min. Ammonia resulting

from the thermal treatment was neutralized using an acidic solution made from equal parts of water and glacial acetic acid. The thermal decomposition process resulted in the PS turning into a dark brown to black powder.

Subsequently, the PS was milled using a Retsch CryoMill from RETSCH GmbH (Haan, Germany) with milling balls of diameters 2 mm and 10 mm, without cooling by liquid nitrogen. Milling was conducted at an oscillation frequency of 20 s^{-1} for 5 min, yielding a fine powder.

2.3. Material Characterization

2.3.1. Nuclear Magnetic Resonance Spectroscopy

^{13}C NMR spectra were acquired via solid-state magic angle spinning (MAS) NMR spectroscopy using an Avance II HD spectrometer from Bruker BioSpin (Rheinstetten, Germany) at a magnetic field strength (B_0) of 7.1 T, employing a spinning rate of 12.5 kHz and a 4 mm triple resonance probe. The acquisition of ^{13}C NMR spectra was conducted through ramped cross-polarization (CP) experiments with a repetition time of 2 s, where the nutation frequency (ν_{nut}) on the proton channel was linearly varied by 50 %. The corresponding ν_{nut} on the ^{13}C channel and the contact time were adjusted to approximately 50 kHz and 1 ms, respectively. Throughout acquisition, including single-pulse and CP, proton broadband decoupling was applied using a spinal-64 sequence with ν_{nut} = 60 kHz. ^{13}C spectra were referenced using the secondary standard adamantane with respect to tetramethylsilane.

^{1}H (500 MHz, D_1 = 1 s) and ^{31}P (202 MHz, D_1 = 5 s) NMR spectra were recorded using a Bruker Avance III HD 500 spectrometer from Bruker BioSpin (Rheinstetten, Germany). Deuterated water was utilized as the solvent. ^{31}P NMR spectra were referenced with respect to 85 % H_3PO_4, set at 0ppm.

2.3.1.1. Fourier-Transform Infrared Spectroscopy: Fourier-transform infrared spectroscopy was conducted using a Nicolet iS50 FTIR spectrometer from Thermo Fisher Scientific Inc. (Waltham, Massachusetts, USA). Each sample underwent an averaging of 128 scans within a wavenumber range spanning from 600 to 4000 cm^{-1} in attenuated total reflection mode.

2.3.1.2. Thermo-Gravimetric Analysis: The thermogravimetric analyses were performed using a Netzsch 209 F1 Libra instrument from Erich Netzsch GmbH & Co. Holding KG (Selb, Germany). For dynamic measurements, the PS samples were heated from 25°C to 1000°C at a constant rate of 10 °Cmin^{-1} under either a nitrogen atmosphere or synthetic air. For isothermal measurements, the PS samples were heated from 25°C to temperatures ranging from 100°C to 180°C at a constant rate of 10 °Cmin^{-1} under a nitrogen atmosphere, and then held at the respective temperature for 30 min. Samples weighing around 10 mg were tested in triplicate.

2.3.1.3. Thermo-Gravimetric Fourier-Transform Infrared Spectroscopy: Thermo-gravimetric Fourier-transform infrared spectroscopy was performed by combining a Mettler Toledo TGA/SDTA 851E from Mettler-Toledo International Inc. (Columbus, Ohio, USA) with a Nicolet iS50 FTIR spectrometer from Thermo Fisher Scientific Inc. (Waltham, Massachusetts, USA). Samples weighing ≈15 mg were subjected to heating from 25°C to 1000°C at a constant rate of 10 °Cmin^{-1} under a nitrogen atmosphere. Volatile degradation products were analyzed every 24 s by averaging 20 scans over a wavenumber range from 400 to 4000 cm^{-1} in transmission mode. To enhance comparability, the intensity profiles were normalized to the sample mass.

2.3.1.4. Differential Scanning Calorimetry: The enthalpy released during GBC (H_{GBC}) and the temperature at which the heat flux peaks ($T_{\dot{Q}_R}$) were determined through dynamic differential scanning calorimetry measurements using a Mettler Toledo DSC 1 instrument from Mettler-Toledo International Inc. (Columbus, Ohio, USA). The measurements were conducted with a heating rate of 10 Kmin^{-1} from 25°C to 280°C. The sample mass was maintained at 1 ± 0.1 mg, and a nitrogen flow rate of 50 mLmin^{-1} was used.

2.3.1.5. Inductively Coupled Plasma Optical Emission Spectroscopy: The phosphorus concentration of the PS was determined via inductively coupled plasma optical emission spectroscopy (ICP-OES) on a Perkin Elmer Optima 2000 DV spectrometer from PerkinElmer, Inc. (Waltham, MA, US). For the measurement, 20 mg sample, 5 mL concentrated nitric acid and 2 mL hydrogen peroxide solution were mixed and were digested at 185°C for 15 min at a heating rate of 8 °Cmin^{-1} in a microwave oven. After cooling, the sample was diluted to 100 mL with deionized water and analyzed by ICP-OES at 213.617 nm. For calibration a commercially available phosphorus standard from Carl Roth GmbH (Karlsruhe, Germany) was used.

2.3.1.6. Influence of the Thermal Decomposition on the Chemical Composition of PS: To better understand the thermal decomposition processes in PS, PS0min was heated in the TGA from 30°C to temperatures between 200°C and 1000°C in 100°C increments. The resulting char was then analyzed using IPC-OES and elemental analysis to correlate specific mass losses in the TGA thermograms with changes in the chemical composition of PS during thermal decomposition. The concentrations of hydrogen, carbon, nitrogen, and sulfur in the PS were determined via CHNS analysis using a UNICUBE instrument from Elementar Analysensysteme GmbH (Langenselbold, Germany). Approximately 2 mg of each sample was pyrolyzed in the presence of a catalytic oxide additive (V_2O_5) at 1150°C. The pyrolysis products were then transported by the carrier gas (He) into the reduction tube and reduced at 850°C. Additionally, by combining the results of ICP-OES and CHNS, and assuming PS consists only of hydrogen, carbon, nitrogen, oxygen, phosphorus, and sulfur, the oxygen content in the PS can be calculated. For simplicity, the specimens in Figure 8 were labeled according to the highest temperature they were exposed to during the TGA.

3. Results and Discussion

3.1. Nuclear Magnetic Resonance Spectroscopy

To evaluate the NMR spectra of PS, spectra of theoretical cyclodextrin model compounds comprising glucose-6-phosphate, glucose-6-diphosphate, and glucose-6-triphosphate, as well as carbamate and urea, were simulated using "Mnova NMR spectra predict 15.0.0" by Mestrelab Research, S.L. (Santiago de Compostela, Spain) (see Supporting Information). To closely match

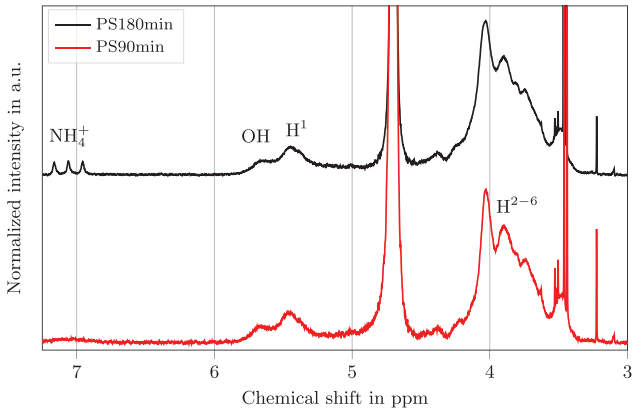

Figure 2. ^{1}H NMR spectra of PS90min and PS180min.

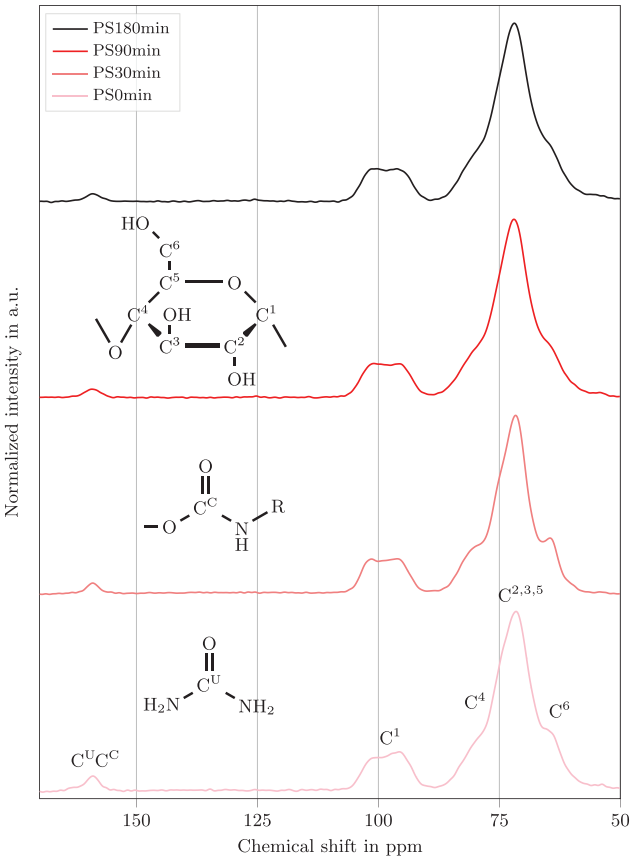

Figure 3. ^{13}C NMR spectra of PS0min, PS30min, PS90min, and PS180min.

the experimental spectra, simulation parameters included a line width of 75 Hz for ^{1}H, 500 Hz for ^{13}C, and 25 Hz for ^{31}P. Deuterium oxide served as the solvent for simulating the ^{1}H spectrum, while deuterated chloroform was selected for both ^{13}C and ^{31}P spectra, as deuterium oxide was unavailable for these simulations. Considering the significant impact of phosphate group protonation on NMR spectra, simulations for the cyclodextrin included two extreme states: complete protonation and deprotonation with ammonia groups as counter-ions.[35,36] Both experimental and simulated NMR spectroscopy data are referenced to identical compounds. To analyze changes in the chemical structure of PS, samples including PS0min, PS30min, PS90min, and PS180min were chosen. These samples offer a comprehensive overview of molecular alterations in PS, representing its state post-synthesis, after minimal heat treatment, midway through the maximum heat treatment duration, and following the full heat treatment period, respectively.

Figure 2 illustrates the ^{1}H NMR spectra of PS90min and PS180min. The spectra for PS0min and PS30min are omitted as they closely resemble those of PS90min but with a lower signal-to-noise ratio. The prominent peak observed at ≈4.7ppm in all ^{1}H spectra corresponds to semi-heavy water, formed via proton exchange with deuterium oxide.[37] Additional peaks at 3.23ppm, 2.10 ppm, 1.79ppm, and 1.11ppm are attributed to water-soluble components of the starch, as determined from measurements of a starch suspension decant. Starch itself exhibits two distinct signal groups: one between 5.80ppm and 5.27ppm, corresponding to OH groups and the H^1 proton, and another between 4.45ppm and 3.37ppm, associated with H^2 to H^6 protons.[38,39] Following heat treatment, a triplet indicative of ammonium ions gradually emerges at 7.08ppm, with an intensity ratio of 1:1:1.[40,41] This emergence is attributed to the decrease in pH resulting from thermal treatment at 160°C, which triggers the decomposition of urea and the elimination of ammonium groups through condensation reactions between ammonium phosphate groups (see Section 3.3). Notably, ammonium ions are only detectable in ^{1}H NMR at a pH value lower than 3.5, with the optimal signal-to-noise ratio observed at a pH value of 2.[41] Otherwise, no significant changes are observed in the spectra due to the thermal treatment. The ^{1}H measurements were conducted in deuterium oxide, leading to the predominant exchange of protons from acid and ammonium groups with deuterons, rendering them barely measurable.

The ^{13}C NMR spectra of PS are presented in **Figure 3**, revealing three distinct signal groups. The first group, spanning between 164ppm and 155ppm, comprises the urea peak at 163ppm and the carbamate group peak at 159ppm.[18] The second and third groups correspond to the carbon atoms of the AGU. Specifically, the C^1 atom displays signals at 101ppm and 96ppm, the C^4 atom at 80ppm, and the C^2, C^3, and C^5 atoms at 72ppm, with the C^6 atom appearing at 65ppm.[42]

Resulting from the heat treatment, urea decomposes into ammonia and isocyanic acid, which subsequently hydrolyzes into ammonia and carbon dioxide, leading to the disappearance of the urea signal. Likewise, the relative intensities of signals corresponding to carbamate groups decrease with longer durations of heat treatment, from 8.33 % for PS0min to 5.94 % for PS30min, and further to 4.33 % for PS180min. However, aside from these changes, the ^{13}C NMR spectra exhibit no detectable alterations due to the heat treatment. This might be attributed to the partial triggering of the GBC during heat treatment, as evidenced in Section 3.3. Furthermore, the comparison between the experimental and simulated ^{13}C NMR spectra of PS reveals excellent agreement, reinforcing the reliability of the simulations.

Figure 4 illustrates the ^{31}P NMR spectra of PS, revealing up to four discernible signals. The first signal, observed between 1.52 ppm and 2.60 ppm, likely corresponds to glucose

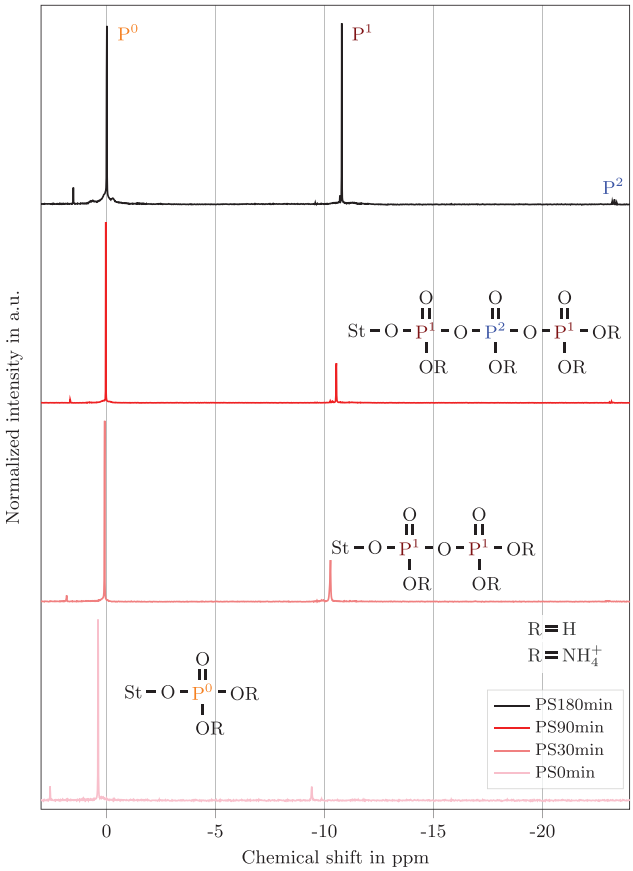

Figure 4. ^{31}P NMR spectra of PS0min, PS30min, PS90min, and PS180min.

6-phosphate, which is released upon GBC.[43] The subsequent signals are identified between 0 ppm and 0.38 ppm, −9.38 ppm to −10.78 ppm, and −22.99 ppm to −23.29 ppm, corresponding to the P^0 atom, the P^1 atom, and the P^2 atom, respectively.[44,45] In this terminology, the superscript number displays the number of P–O–P bonds a P atom has, i.e. P^0 is a monophosphate, P^1 a diphosphate, and P^2 a polyphosphate (see Figure 4).

The relative intensities of the signals corresponding to different phosphate functional groups undergo significant changes due to prolonged heat treatment of PS. Initially, the signal intensity attributed to the P^0 atom (0.38 ppm) is maximal for PS0min, indicating the prevalence of ammonium monophosphate esters following the phosphatization step of synthesis. Simultaneously, the presence of ammonium diphosphate esters in PS0min is confirmed by the signal corresponding to the P^1 atom at −9.38 ppm. Upon heat treatment, the signals corresponding to glucose-6-phosphate, the P^0, and P^1 atoms of PS30min shift upfield to 1.83 ppm, 0.08 ppm, and −10.28 ppm, respectively. This shift likely arises from changes in the degree of protonation and thus in pH value, which significantly influences phosphate group chemical shifts. Blennow's and Maki's groups found that the chemical shift of glucose-6-phosphate or triphosphate esters and thus of the P^0, P^1 and P^2 atoms changes by around 4 ppm between a pH value of 4 and 9.[35,36] Subsequently, the measured signals shift due to urea decomposition and condensation of ammonium phosphate groups, releasing ammonia in both reactions and lowering the sample's pH value. With prolonged heat treatment, the signals continue shifting upfield, and the signal corresponding to the P^1 atom increases from 7.3 % for PS0min to 22.9 % for PS30min. At −23.17 ppm, a triplet corresponding to the P^2 atom gradually emerges, indicating condensation reactions between ammonium phosphate esters, and polyphosphate formation via ammonium mono- and diphosphate ester condensation. In accordance with TGFTIR results (see Section 3.3), showing that ammonia and water are released upon temperature increase, it can be assumed that a reaction similar to the decomposition of ammonium polyphosphate takes place.[47] In the ^{31}P NMR spectrum of PS180min, increased signals for the P^1 and P^2 atoms are observed due to condensation reactions between ammonium phosphate esters, with P^1 becoming the dominant signal while P^0 decreases to 98.6 %. Notably, shoulders gradually emerge next to the main signals corresponding to the P^0 and P^1 atoms, likely indicating phosphatization at all three hydroxyl groups of the AGU. Steric considerations favor phosphatization at the C^6 atom, explaining the largest signal (−0.01 ppm). Phosphatization at the C^2 atom is preferred due to its higher acidity compared to the C^3 atom, resulting in the second-highest signal (−0.29 ppm, 3.2 %), while the C^3 atom shows the smallest signal (0.62 ppm, 2.0 %).[48] This phosphatization of the hydroxyl groups of the C^2 and C^3 atoms may occur via secondary phosphatization by ammonium phosphate groups separated during heat treatment. The implications of such separation on PS's thermal stability and GBC are detailed in Section 3.3. **Table 1** compares the ^{31}P NMR spectra results with those of this study, revealing moderate chemical shift differences. The measured spectrum aligns more closely with the spectrum of completely deprotonated phosphates, reinforcing arguments for the existence of ammonium phosphate esters.

Table 1. Chemical shifts of P^0, P^1, and P^2 atoms of PS180min compared to literature.

Study	P^0 in ppm	P^1 in ppm	P^2 in ppm
Rothenhäusler and Ludik et al.	0	−10.8	−23.3
Heinze et al.[18]	3.3	−8	−20
Passauer et al.[19]	1.3	−1–0	
Fiss et al.[44]	0.3	−12	
Kröger et al.[45]	1.4	−8.3	
Azeroual et al.[46]	2	−10	

In summary, prior to heat treatment, PS contains residual urea, carbamate-type functional groups, as well as ammonium monophosphate esters and monophosphoric amides, along with some ammonium diphosphate esters. As the heat treatment progresses post-phosphatization, several changes occur: residual urea is eliminated, thermally unstable carbamate-type groups decompose, and the ammonium phosphate esters condense into ammonium polyphosphates (see **Figure 5**).

3.2. Fourier-Transform Infrared Spectroscopy

The functional groups present in unmodified wheat starch (WS), PS without additional heat treatment after synthesis (PS0min),

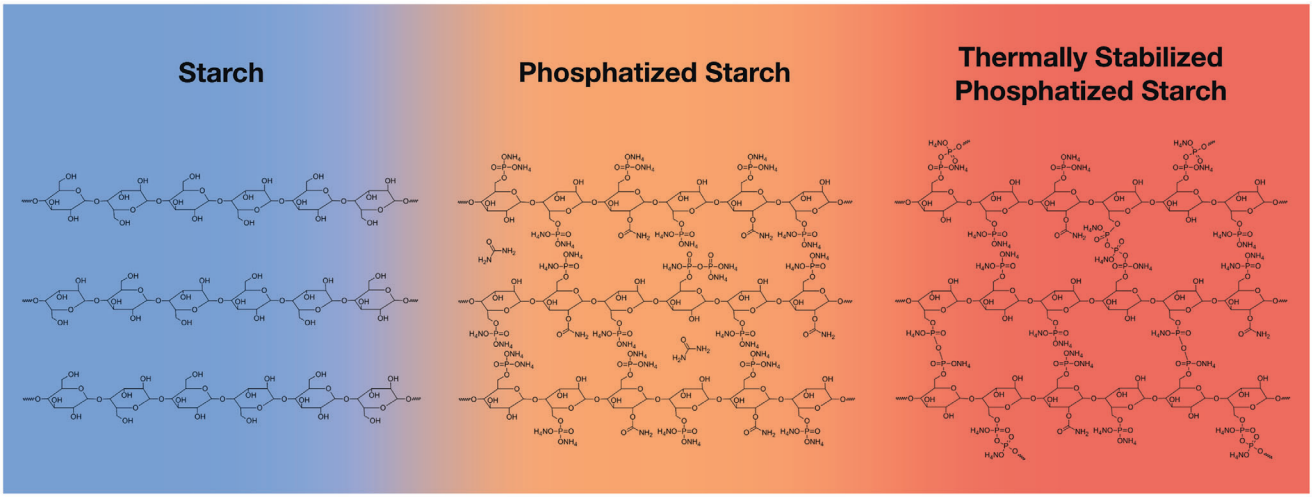

Figure 5. Chemical structures of starch, PS, and thermally stabilized PS.

and PS subjected to the maximum duration of heat treatment at 160°C (PS180min) were analyzed using FTIR spectroscopy. Both WS and PS exhibit characteristic peaks typical of polysaccharides, corresponding to vibrations of the OH, CH, C-O-C, and C-O-H groups (see **Table 2**). However, the functional groups introduced in PS as a result of its modification with urea and phosphoric acid overlap with the peaks observed in WS. A new peak emerges at 1700 cm^{-1}, corresponding to the C = O group of urea and various carbamate-type groups (see Figure 1). Similarly, the P = O vibration is observed at 1150 cm^{-1}, while peaks resulting from P-O-C and P-O-H groups are found at 1020 cm^{-1} and 920 cm^{-1}, respectively. In contrast to the NMR results, there is no significant difference between the FTIR spectra of PS0min and PS180min (**Figure 6**).

Table 2. Wavenumbers and the corresponding band assignments of the FTIR spectra of WS and PS.

Sample	Wavenumbers in cm^{-1}	Band assignment
WS	3300	O-H stretching[49]
	2930	CH_2 antisymmetric stretching[50,51]
	2900	CH_2 symmetric stretching[50,51]
	1640	C-O bending associated with OH group[52]
	1415	CH_2 symmetric scissoring[53]
	1335	CH, CH_2 deformation[54]
	1245	CH, CH_2 deformation[53]
	1210	CH, CH_2 deformation[54]
	1150	C-O-C α-1,4 glycosidic linkage[55]
	1080	C-O-H[55]
	995	C-O-C α-1,4 glycosidic linkage[55]
	930	C-O-C α-1,4 glycosidic linkage[55]
	860	C-O-C ring mode[55]
	760	CH_2[55]
PS	3190	N-H stretching[56]
	2920	CH_2[50]
	1700	C = O Urea, Carbamate[18]
	1650	C-O bending associated with OH group[52]
	1440	CH[57]
	1250	CH, CH_2 deformation[53]
	1150	P = O, C-O-C α-1,4 glycosidic linkage[55,58]
	1020	P-O-C, C-O-C α-1,4 glycosidic linkage[55,59,60]
	920	P-O-H, C-O-C α-1,4 glycosidic linkage[26,55]

3.3. Thermo-Gravimetric Analysis and Thermo-Gravimetric Fourier-Transform Infrared Spectroscopy

Upon elucidating the molecular structure of PS and its alterations during post-synthesis heat treatment via NMR spectroscopy, the ensuing discourse delves into the thermal stability and decomposition mechanisms of PS. This necessitates a simultaneous elaboration of the TGA thermograms of PS after various heat treatment durations (see **Figure 7**), the corresponding FTIR

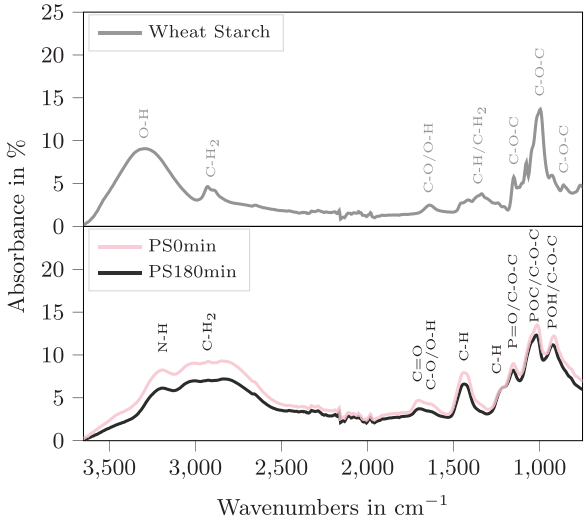

Figure 6. FTIR spectra of wheat starch, PS0min and PS180min.

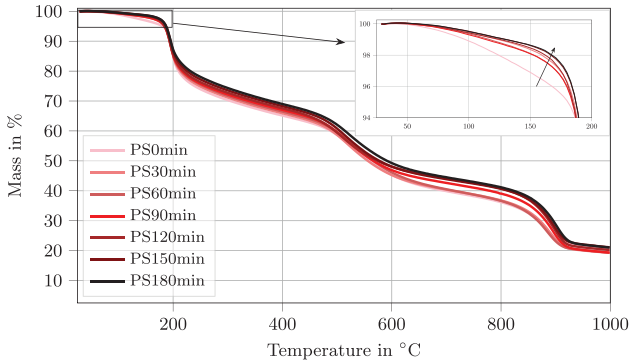

Figure 7. TGA thermograms of PS under nitrogen after different periods of heat treatment at 160°C.

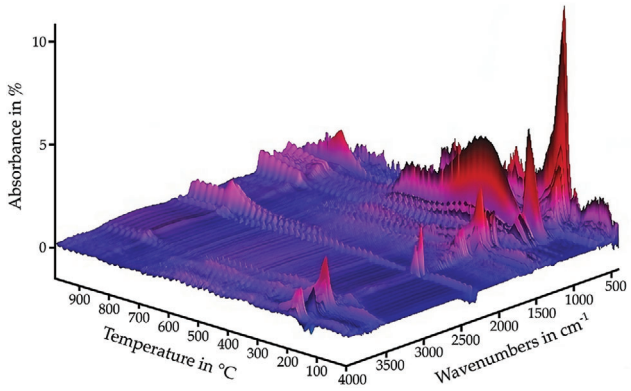

Figure 9. TGFTIR spectra of PS30min.

spectra derived from TGFTIR analysis (see Figures 9 and 10), and changes in the chemical composition PS0min resulting from its decomposition (see **Figure 8**). Special emphasis is placed on the absorbance-temperature profiles observed at distinct wavenumbers: 965 cm^{-1} (indicative of ammonia), 420 cm^{-1} (potentially associated with hydrocarbons), 2310 cm^{-1} (representative of carbon dioxide), 2180 cm^{-1} (corresponding to carbon monoxide), 1250 cm^{-1} (associated with P = O bonds), and 715 cm^{-1} (potentially indicative of P-N-C or C-N-C bonds). It is imperative to acknowledge a certain temporal discrepancy between the initiation of PS decomposition, the liberation of low molecular weight compounds leading to weight loss as detected by TGA, and the subsequent detection of these volatile species via FTIR. In the interest of clarity, the discussion initially centers on measurements conducted under a nitrogen atmosphere, prior to an examination of the impact of oxygen on the thermal decomposition of PS (refer to Figure 13).

The TGA thermograms depicted in Figure 7 illustrate the thermal decomposition behavior of PS following various durations of heat treatment at 160°C, as outlined in Section 2.2. Before delving into the impact of different heat treatment durations on PS, it is advisable to provide a general overview of the TGA thermograms. PS exhibits multiple decomposition stages upon elevation of temperature. First, there is a mass loss observed up to 100°C, attributed to the evaporation of water attracted to the hydroxyl groups of the AGU within the PS structure.[61] This is substantiated by several peaks spanning the wavenumber ranges of 3400 to 4000 cm^{-1} and 1300 to 1800 cm^{-1}, alongside a prominent peak at 1630 cm^{-1}, as depicted in **Figure 9**.[62]

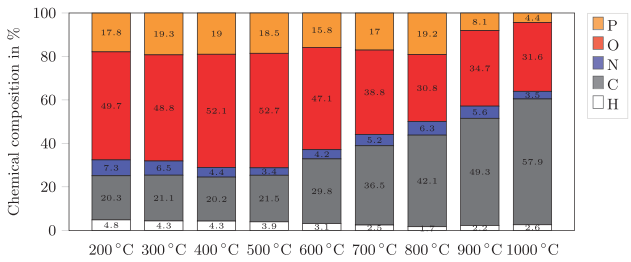

Figure 8. Chemical composition of PS0min after pyrolysis at temperatures between 200°C to 1000°C in the TGA.

The subsequent stage involves a reduction in mass up to 170°C, attributable to diverse chemical reactions such as the decomposition of carbamate groups and the consequent liberation of ammonia.[63,64] The presence of ammonia is readily discernible in the FTIR spectra by two pronounced peaks at 925 cm^{-1} and 965 cm^{-1}, accompanied by various peaks between 800 cm^{-1} and 1200 cm^{-1}, alongside a weaker peak at 3330 cm^{-1} (refer to Figure 9).[62] This process coincides with the decomposition of urea into ammonia and isocyanic acid.[65] Passauer et al. noted a peak at 2250 cm^{-1}, corresponding to the N═C═O stretching vibration of isocyanic acid during TGFTIR of PS.[62,66] Notably, there are no significant readings for PS0min and only noise for PS30min and PS180min at the same wavenumbers.

Concurrently, condensation reactions leading to the liberation of water and ammonia occur across a broad temperature range, significant up to 600°C.[25] Plausible mechanisms entail condensation reactions involving ammonium phosphate groups and phosphate groups. As elucidated in Section 3.1, the relative intensities of diphosphate esters and triphosphate esters notably increase with prolonged heat treatment at 160°C. Since residual phosphoric acid is absent post PS synthesis and purification, the formation of ammonium di- and triphosphate esters must stem from condensation reactions between ammonium monophosphates, ammonium mono- and diphosphate esters, respectively. Consequently, water and ammonia are liberated, while new P-O-P bonds are formed, akin to the thermal decomposition of ammonium polyphosphate (APP).[47,67] Camino et al. demonstrated that ammonia release resulting from condensation reactions during the thermal decomposition of APP persists up to 600°C, consistent with **Figure 10** (a).[47] The intensified peak at 965 cm^{-1} confirms the release of ammonia as a consequence of the aforementioned mechanisms. Intriguingly, the FTIR peaks corresponding to ammonia and water both diminish around 600°C, further supporting the previously outlined decomposition mechanism.[68]

It is imperative to reiterate that the discussed condensation mechanisms invariably yield highly cross-linked PS, wherein AGU are not only linked to their neighboring AGU of the same amylose molecule via ether bonds but also connected to the AGU of other amylose molecules via various functional groups.[46,69] The released ammonia and water substantially

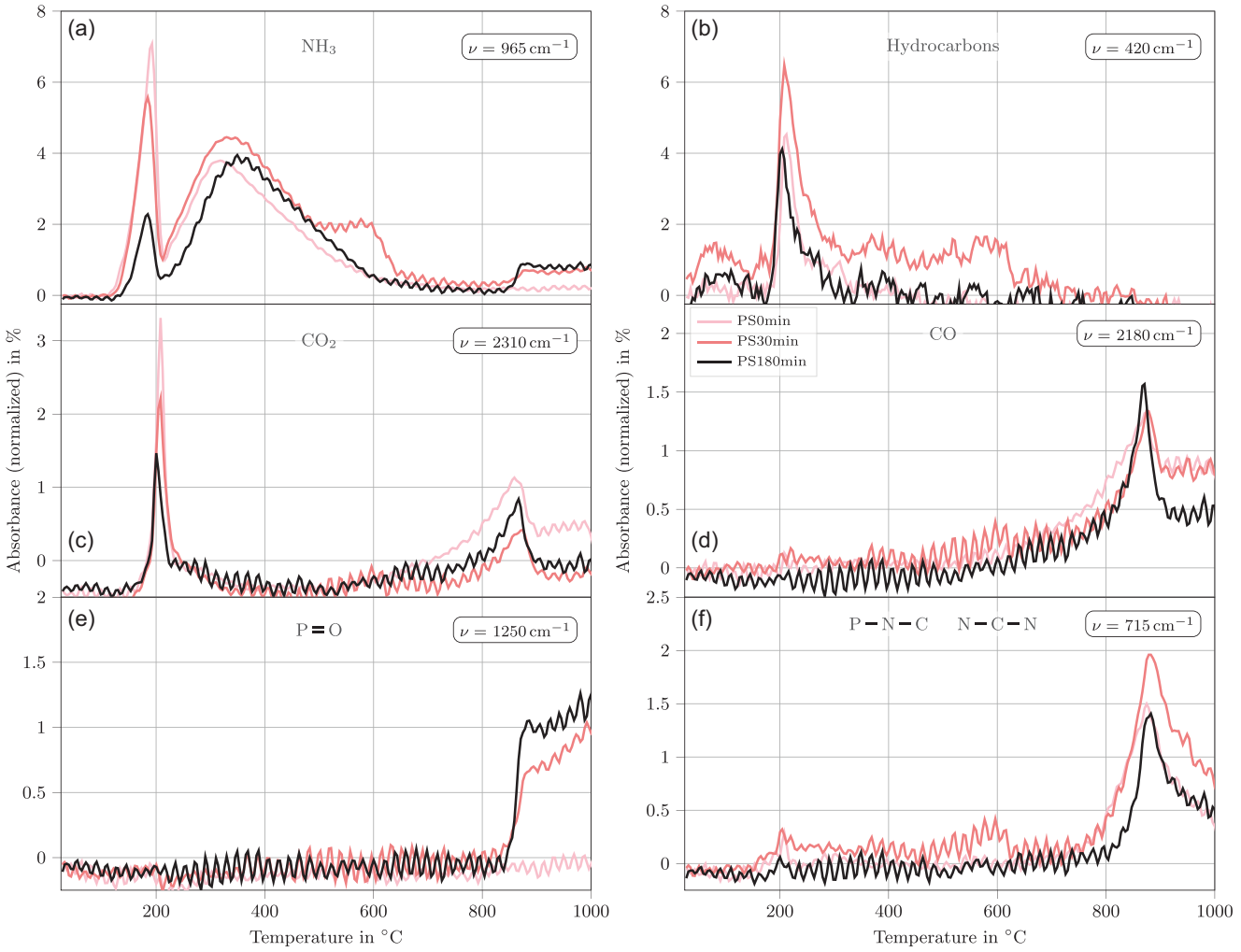

Figure 10. Absorbance-temperature profiles at wavenumbers of 965 cm^{-1} (a), 420 cm^{-1} (b), 2310 cm^{-1} (c), 2180 cm^{-1} (d), 1250 cm^{-1} (e), and 715 cm^{-1} (f) from TGFTIR of PS0min, PS30min, and PS180min.

contribute to the flame retardancy of PS by diluting the flame zone with non-combustible gases and diminishing the combustion efficiency.[10,70]

Following the aforementioned stages, a gradual decrease in mass is succeeded by a sharp mass loss commencing at approximately 170°C, signifying GBC. This entails the fragmentation of the starch backbone through the rupture of ether bonds between AGU, yielding anhydrosugars such as levoglucosan which are subsequently dehydrated.[71–73] During this process, a rapid succession of chemical reactions occurs, yielding a diverse array of viscous and volatile decomposition products.[74–76] Alongside anhydrosugars, aldehydes, furanoid, and pyranoid compounds are generated and partially released alongside volatile compounds like CO, CO_2, H_2O, and CH_4.[77,78] Zhang et al. demonstrated that the char of starch post thermal decomposition primarily comprises phenol, benzene, and furan-like structures bonded via methylene or ether bonds.[79]

Ji et al. investigated the char of PS using FTIR and demonstrated that pyrolysis of PS at 250°C results in a crosslinked, phosphate-containing, and carbonized starch.[24] Considering the pyrolysis products of native starch, it is plausible that the GBC of PS results in crosslinked aromatics that are functionalized, among other things, with ammonium phosphates. Based on current knowledge of their molecular structure, the pyrolysis products of PS in the temperature range of the GBC could be described as phosphatized polyaromatics (PPA). To date, the potential of PPA as FR has not yet been scientifically explored. However, the molecular structure, thermal decomposition behavior, and chemical composition of PPA play a key role in understanding the flame retardancy of PS.

GBC in unmodified starches typically occurs at around 300°C, contingent upon the starch's source and amylose content.[80–82] Phosphorus-containing FR can act as acid catalysts in the condensed phase, inducing charring through esterification and dehydration in temperature ranges preceding the decomposition of the original materials.[83,84] This elucidates why GBC occurs in PS at ≈130°C lower temperatures compared to unmodified starch.[85] During this process, PS experiences a mass loss of around 15%, leaving ≈ 80 to 85% residual mass at 220°C. This contrasts sharply with unmodified starch, which typically

retains around 20 % residual mass post GBC, contingent upon the starch's source and amylose content.[86] Passauer et al. concluded that the disparity in mass loss due to GBC between unmodified starch and PS might be attributed to the influence of phosphate and ammonium phosphate groups on the condensed phase.[62] These groups induce phenomena such as acid-catalyzed dehydration, esterification, cross-linking, and aromatization.[87,88]

Resulting from the decomposition of residual urea, thermally less stable carbamate groups, and the GBC, the chemical composition of PS0min changes. Since no phosphorus is released during these decomposition reactions, its concentration increases from 15.2 % to 17.8 % (see Figure 8). In contrast, the concentrations of hydrogen and nitrogen decrease by the release of ammonia. Notably, the intensity-temperature profiles resulting from TGFTIR of ammonia and water exhibit heightened intensities at much lower temperatures than that of the GBC (T_{GBC}). However, in contrast to water, the FTIR peaks corresponding to ammonia abruptly decline at T_{GBC}. Passauer et al. observed a similar trend during their thermal characterization of ammonium starch phosphate carbamates but did not provide insight into why this phenomenon might occur.[62]

Two plausible explanations arise: a) the release of ammonia is abruptly stopped precisely at T_{GBC}, or b) the ammonia released during T_{GBC} is consumed in the manifold reactions occurring during GBC. The abruptness of the intensity-temperature profile drop lends credence to the latter explanation. However, the specific reactions in which ammonia participates remain unclear. One conceivable reaction may involve the incorporation of ammonia during the secondary phosphatization of PS, akin to the synthesis of APP.[89,90] The peaks corresponding to CO_2 and water reach their maximum during GBC, while no CO was detected (see Figure 10c,d).[62] Additionally, the peak at 420 cm^{-1}, accompanied by peaks at 400 cm^{-1} and 450 cm^{-1}, also undergoes a significant increase at T_{GBC}, potentially corresponding to hydrocarbons (see Figure 10b). However, without additional analysis techniques such as gas chromatography and mass spectrometry, this assumption must be approached cautiously.

Following GBC, the mass of PS gradually decreases with increasing temperature, accompanied by the release of water and ammonia. Condensation reactions involving functional groups, such as ammonium phosphate, are likely responsible for the continuous release of water and ammonia up to approximately 600°C. This results in a decrease of the concentration of hydrogen and nitrogen, and a slight increase in the phosphorus content up to 400°C. However, there is a drop in the phosphorus concentration between 400°C and 600°C which is akin to the thermal decomposition of APP. At this temperature, the residual mass of PS typically ranges between 45 to 50%. Subsequently, between 600°C and approximately 800°C, a slow mass loss occurs, attributed to an increased release of CO and CO_2, indicating the aromatization and graphitization of PS during its decomposition. (see Figure 10c,d). In this temperature range, the oxygen concentration in PS0min decreases from 47.1 % to 30.8 % while the carbon concentration increases from 29.8 % to 42.1 %. A steep decline in mass occurs at around 900°C, resulting in a residual mass of approximately 20 % at 1000°C, thus aligning with the residual mass of unmodified starch.

Although unmodified starch achieves a similar residual mass shortly after GBC, PS undergoes multiple decomposition steps post-GBC. The incorporation of phosphorus enhances the thermo-oxidative stability of the char at high temperatures, thereby contributing to the increased residual mass of PS.[91] The final mass loss coincides with elevated signals for CO and CO_2. Simultaneously, significant increases are observed in the absorbance-temperature profiles at 965 cm^{-1} and 1250 cm^{-1} of PS30min and PS180min, corresponding to ammonia and P = O, respectively (see Figure 10a,e).[84] The steep mass loss at around 900°C is accompanied by a significant decrease in the phosphorus concentration, agreeing with the TGFTIR absorbance-temperature profiles of PS30min and PS180min at 1250 cm^{-1}. This indicates that the polyphosphates decompose and PO radical-forming compounds are released, which was not detected in previous investigations.[25,62] Simultaneously, the carbon concentration increases from 42.1 % at 800°C to 57.9 % at 1000°C, suggesting further aromatization and graphitization of the PS.

Figure 9 illustrates the aforementioned vibration bands as well as the distinct vibration bands between 950 to 1200 cm^{-1} resulting from P-O-C and P-O-H groups. PO radicals originating from these groups significantly contribute to the flame retardancy of PS by inhibiting flames through radical scavenging of H and OH radicals in the flame zone.[92] Intriguingly, another peak emerges at 715 cm^{-1} at around 800°C, following the peaks corresponding to CO and CO_2 but preceding those of ammonia and P = O. Shao et al. argued during their investigation of the thermal decomposition mechanisms of APP modified with ethanolamine that the peak at 720 cm^{-1} corresponds to the formation of P-N-C bonds, consistent with findings by Camino et al.[47,93,94] Alternatively, the presence of C-N-C bonds akin to urea may account for the peak at 715 cm^{-1}.[95]

Comparing the TGA thermograms of PS for different heat treatment durations reveals a trend wherein the mass loss between room temperature and 100°C decreases with increasing heat treatment periods, diminishing from 1 % for PS0min to 0.5 % for PS180min. This initial mass loss primarily arises from the physical drying of PS and the evaporation of water. Upon further temperature elevation to 150°C, PS0min experiences an additional mass loss of approximately 2.1 %, whereas PS180min exhibits a reduced loss of around 0.9 %. This decline in mass loss within the same temperature range can be attributed to the preceding decomposition of urea and the ceasing of condensation reactions, which are no longer initiated during TGA following the heat treatment at 160°C. The onset of ammonia release occurs at higher temperatures for longer periods of heat treatment (see Figure 10a). Concurrently, there is a significant reduction in the intensity of peaks at 965 cm^{-1}. Since the mass loss arises from the evaporation of volatile decomposition products, there is a significant reduction in the risk of pore formation at elevated temperatures during the processing of thermoplastics and thermosets.

During GBC, there is a noticeable reduction in the intensity of the peak corresponding to CO_2 at 2310 cm^{-1} with increasing periods of heat treatment at 160°C. This reduction in CO_2 readings suggests that GBC may be partially initiated during the heat treatment, leading to decreased CO_2 emissions. This observation suggests the potential to enhance the thermal stability of PS by incorporating GBC as part of a further modified synthesis

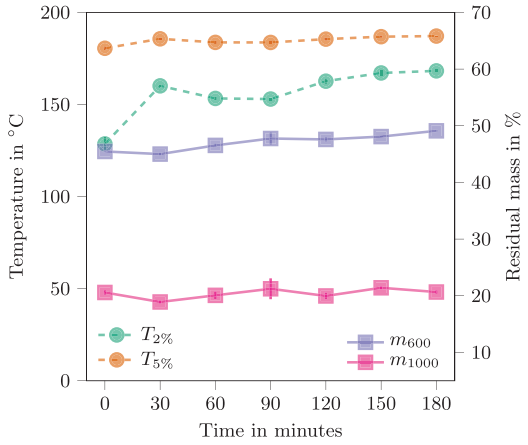

Figure 11. $T_{2\%}$, $T_{5\%}$, m_{600}, and m_{1000} resulting from TGA of PS under nitrogen after different periods of heat treatment at 160°C.

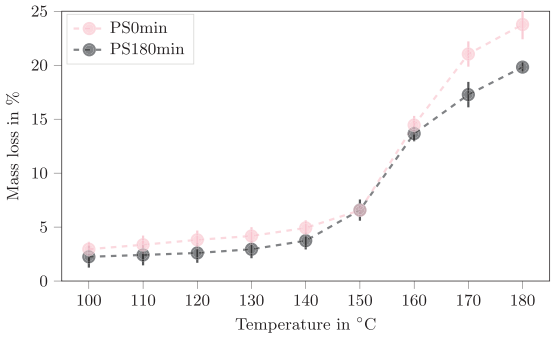

Figure 12. Mass loss resulting from isothermal TGA measurements of PS0min and PS180min at temperatures between 100°C and 180°C for 30 min.

procedure. As a result, the onset of decomposition would not be solely determined by GBC, but rather by the temperature at which the formation of ammonium polyphosphates triggers an increased release of ammonia and water. Following GBC, the TGA thermograms of PS with varying heat treatment durations generally exhibit similar trends. The residual mass of PS increases with longer heat treatment periods up to 1000°C.

The TGA thermograms depicted in Figure 7 are further analyzed in **Figure 11**, which illustrates the temperature at which 2 % mass loss occurred ($T_{2\%}$), the temperature at which 5 % mass loss occurred ($T_{5\%}$), and the residual masses at 600°C (m_{600}) and at 1000°C (m_{1000}) of the PS after varying periods of heat treatment at 160°C. The $T_{2\%}$ exhibits a gradual increase from 128.6°C for PS0min, plateauing at approximately 168.3°C for PS180min, indicating an enhancement in thermal stability within this temperature range with prolonged heat treatment periods. This elevation in $T_{2\%}$ is likely attributable to the initiation of condensation reactions and the decomposition of residual urea within the PS, as previously discussed. In contrast, the $T_{5\%}$ shows a narrower increase, rising marginally from 180.5°C to 187.2°C, indicating that T_{GBC} remains unaffected by the heat treatment at 160°C. The m_{600} increases from 45.5 % for PS0min to 49.1 % for PS180min, while m_{1000} remains around 20 % irrespective of the duration of heat treatment. This elevation in m_{600} can be attributed to the heightened phosphorus content of PS, which increases from approximately 15.2 % for PS0min to about 16.5 % for PS subjected to heat treatment. Additionally, the observed increase in m_{600} may be influenced by the aforementioned condensation reactions that have already occurred.[91]

Polymer processing entails prolonged exposure to elevated temperatures, making it imperative to evaluate the thermal stability of PS under such conditions. Isothermal TGA measurements are conducted across temperatures ranging from 100°C to 180°C, as depicted in **Figure 12**. Substantial differences in mass loss become apparent even at modest temperatures such as 100°C. Below 140°C the mass loss ranges from approximately 2.2 to 4.2%. However, a notable increase in mass loss occurs around 150°C, signaling the onset of GBC. Beyond this threshold, the rate of mass loss gradually aligns with that observed during dynamic TGA measurements subsequent to GBC. As previously highlighted, the diminished mass loss at temperatures necessary for polymer processing significantly mitigates the risk of pore formation. Moreover, given that the glass transition temperature of epoxy resin-based thermosets typically spans a narrow temperature range around the maximum curing temperature, increasing the upper limit of the curing temperature enables the curing of epoxy resins and curing agents with a higher potential glass transition temperature, thereby enhancing overall mechanical performance.[96,97] Nevertheless, it is crucial to acknowledge that the maximum curing temperature is constrained by the T_{GBC} of the PS (140°C). This limitation underscores the necessity for a meticulous understanding of the thermal properties of PS in the context of polymer processing to optimize processing conditions and material performance effectively.

The extensive discussion of the thermal decomposition mechanisms in PS under anaerobic conditions can be summarized as follows:

a) Decomposition of thermally unstable carbamate groups, resulting in the release of ammonia.
b) Decomposition of residual urea, leading to the generation of ammonia and isocyanic acid, which further hydrolyzes into CO_2 and ammonia.
c) Condensation reactions between ammonium phosphate groups, releasing water and ammonia.
d) GBC triggered by the release of acid functionalities, accompanied by the release of CO_2 and water, while the production of ammonia is reduced.
e) Aromatization and graphitization of the PS, resulting in the release of CO and CO_2.
f) Decomposition of phosphate functional groups, releasing PO-type compounds.

Following the examination of the thermal stability and thermal decomposition mechanisms of PS under an inert nitrogen atmosphere, the discussion now shifts to the TGA thermograms of PS in a synthetic air environment, as illustrated in **Figure 13**. Notably, GBC initiates at slightly lower temperatures in synthetic air compared to nitrogen, approximately 5°C lower. Similar to the

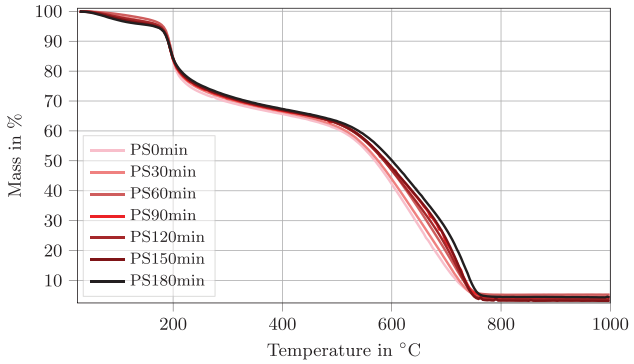

Figure 13. TGA thermograms of PS in synthetic air after different periods of heat treatment at 160°C.

trends observed in Figure 7, PS subjected to longer periods of heat treatment exhibits higher residual masses post-GBC. Up to 500°C, the TGA thermograms of PS in both nitrogen and synthetic air exhibit analogous patterns. However, beyond 500°C, while PS undergoes distinct decomposition steps in nitrogen, decomposition in synthetic air occurs more gradually between 500°C and 750°C, resulting in residual masses of only a few percent. This discrepancy suggests that the decomposition of ammonium phosphate groups is instigated at lower temperatures in synthetic air, thereby enhancing the gas phase activity of PS under aerobic conditions. The residual mass observed at 1000°C may potentially stem from the formation of polyphosphate-based inorganic glasses.[62]

3.4. Differential Scanning Calorimetry

As explored in the preceding section, the heating of PS initiates numerous physical and chemical reactions, yielding various endothermal and exothermal heat fluxes, notably highlighted by the exothermal heat flux during GBC. This phenomenon is characterized by two key parameters: the temperature of the maximum heat flux ($T_{\dot{Q}_P}$) and the enthalpy of the exothermal reaction (H_{GBC}), as depicted in **Figure 14**. Observations reveal a subtle shift in $T_{\dot{Q}_P}$ towards slightly lower temperatures with increasing periods of heat treatment, ranging from 202.7°C for PS0min to 199.6°C for PS180min. This trend aligns with findings by Passauer et al., attributing the shift to a heightened degree of modification.[62]

The enthalpy released during GBC ranges from $-68.7\ Wg^{-1}$ to $-83.5\ Wg^{-1}$. The absolute value of H_{GBC} tends to decrease with prolonged heat treatment periods. This observation corresponds with the trends observed in Figure 10a,c, indicating decreased ammonia and CO_2 peaks with increased heat treatment periods. Both phenomena likely stem from partially triggered condensation reactions and GBC, resulting in reduced gas emissions and, consequently, a decrease in H_{GBC}.

4. Conclusion and Outlook

A modified synthesis approach for PS is introduced, and its impact on the molecular structure, thermal stability and thermal decomposition mechanisms of PS are investigated. Elevated heat treatment beyond the conventional 135°C used in PS synthesis induces several molecular alterations: first, the residual urea is eliminated as evidenced by the ^{13}C NMR spectra. Second, the C^2 and C^3 of the AGU undergo phosphatization in a secondary phosphatization reaction, as evidenced by shoulders in the ^{31}P NMR spectra. Third, monophosphate esters and diphosphate esters give rise to increased formation of diphosphate and new polyphosphate esters, facilitating cross-linking of the PS. Phosphatization yields various functional groups with overlapping vibration bands akin to the WS, although no discernible differences are observed in the FTIR spectra of PS0min and PS180min. Thermal decomposition mechanisms of PS are meticulously analyzed via TGFTIR up to 1000°C, identifying volatile decomposition products and hypothesizing corresponding molecular changes in PS.

This study marks the first instance of detecting P = O type compounds as PS decomposition products via TGFTIR. Possible flame retardant mechanisms in the condensed phase might involve acid-catalyzed dehydration, cyclization, cross-linking and aromatization. Corresponding possible gas-phase mechanisms might include flame zone dilution with non-combustible gases (ammonia and water) and flame inhibition via radical scavenging by PO radicals. Isothermal TGA measurements assess the thermal stability for polymer processing, revealing significantly enhanced thermal stability, and delayed and reduced release of volatile compounds, enabling PS processability in bulk materials up to 140°C. DSC demonstrates a shift in $T_{\dot{Q}_P}$ to slightly lower temperatures due to increased phosphorus-content resulting from heat treatment, possibly partially triggering GBC and leading to decreased H_{GBC}.

By comprehensively evaluating molecular structural changes in PS resulting from heat treatment, and its decomposition mechanisms during TGA, avenues for further enhancing the thermal stability of PS are explored. Subsequent studies will investigate the potential of PPA as FR for polymers requiring processing temperatures exceeding T_{GBC}. Furthermore, the improved processability of PS through the modified synthesis route prompts investigation into its flame retardancy in epoxy resins, marking a pioneering application of PS as an FR in polymeric bulk materials.

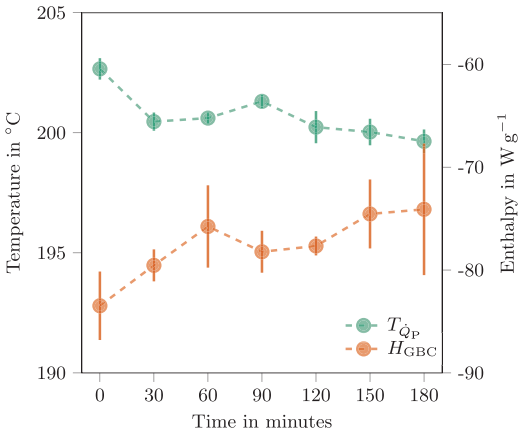

Figure 14. Temperature at which the heat flux is maximal $T_{\dot{Q}_P}$ and the enthalpy released during the GBC H_{GBC} of PS after different periods of heat treatment at 160°C.

Acknowledgements

The authors want to thank Ute Kuhn for her support during the experiments. Further thanks goes to Dr. Ulrike Lacher from the Department of Organic Chemistry I for providing the ^{31}P-spectra. The authors are grateful to the North Bavarian NMR Center (NBNC) for providing access to the NMR spectrometers used for both solid-state and solution NMR spectroscopy. We would like to thank all colleagues of the work group "Resins & Composites" at the Department of Polymer Engineering for their support. Parts of the research documented in this manuscript have been funded by the German Federal Ministry for Economic Affairs and Climate Action (BMWK) within the research projects "EcoPrepregs - Grundlagenforschung zur Klärung der Struktur-Eigenschaftsbeziehungen von Epoxidharzen und Fasern aus nachwachsenden Rohstoffen zur Anwendung in der Sekundärstruktur von Flugzeugen" (grant # 20E1907A, Germany) and "NewPreg - Nachhaltige, wirtschaftliche und funktionalisierte Bio-Feststoffharz-Prepregtechnologie zur CO_2-Reduktion durch kühlfreie Lagerung, Einsatz erneuerbarer Ressourcen und Gewichtsreduktion durch maßgeschneidertes Drapierverhalten" (grant # 20Q2227C, Germany).

Open access funding enabled and organized by Projekt DEAL.

Conflict of Interest

The authors declare no conflict of interest.

Data Availability Statement

The data that support the findings of this study are available from the corresponding author upon reasonable request.

Keywords

bio-based, flame retardant, phosphatized starch, sustainability

Received: July 15, 2024
Revised: November 29, 2024
Published online: February 28, 2025

[1] A. K. Chaturvedi, D. C. Sanders, *Aviat. Space Environ. Med.* **1996**, *67*, 275.
[2] R. Peacock, R. Bukowski, W. Jones, P. Reneke, V. Babrauskas, J. Brown, Fire safety of passenger trains, Technical report, U.S. Department of Transportation /Federal Railroad Administration, **1993**.
[3] E. M. S. Agency, Annual overview of marine casualties and incidents 2022, Technical report, European Maritime Safety Agency, **2022**.
[4] M. R. S. Henri Vahabi, G. Malucelli, *Analysis of Flame Retardancy in Polymer Science*, Elsevier, Amsterdam, **2022**.
[5] A. D. Blum, L. Birnbaum, R. Weber, K. Kannan, D. Rich, D. Lucas, C. Koshland, D. Dobrace, S. Hanson, *Rev. Environ. Health* **2010**, *25*, 261.
[6] S. Kemmlein, D. Herzke, R. J. Law, *J. Chromatogr. A* **2009**, *1216*, 320.
[7] National Research Council (US) Subcommittee on Flame-Retardant Chemicals, *Toxicological Risks of Selected Flame-Retardant Chemicals*, National Academies Press (US), Washington (DC), **2000**.
[8] J. Green, *J. Fire Sci.* **1992**, *10*, 470.
[9] B. Schartel, *Materials* **2010**, *3*, 4710.
[10] M. M. Velencoso, A. Battig, J. C. Markwart, B. Schartel, F. R. Wurm, *Angew. Chem., Int. Ed.* **2018**, *57*, 10450.
[11] J. Hastie, *J. Res. Natl. Bureau Standards. Sec. A, Phys. Chem.* **1973**, *77*, 733.
[12] K. Salmeia, J. Fage, S. Liang, S. Gaan, *Polymers* **2015**, *7*, 504.
[13] C. D. Papaspyrides, P. Kiliaris, *Polymer green flame retardants*, Newnes, **2014**.
[14] S. Huo, P. Song, B. Yu, S. Ran, V. S. Chevali, L. Liu, Z. Fang, H. Wang, *Prog. Polym. Sci.* **2021**, *114*, 101366.
[15] L. Passauer, S. Fischer, H. Bender, S. Tech, A. Wagenführ, Use of water-soluble nitrogen- and phosphorus-containing polysaccharide derivatives as flame retardants, wood composite material with improved flame retardance properties and process for its preparation, **2012**, https://patents.google.com/patent/DE102012204238B4/en, DE102012204238B4.
[16] L. Passauer, S. Fischer, H. Bender, S. Tech, A. Wagenführ, Flame retardants comprising polysaccharide derivatives containing nitrogen and phosphorus and use thereof to improve the flame-retardant properties of wood and wood composite materials, **2013**, https://patents.google.com/patent/EP2825615A1/en, EP2825615A1.
[17] J. F. Robyt, *Starch: Structure, Properties, Chemistry, and Enzymology*, Springer Berlin Heidelberg, Berlin, Heidelberg, ISBN 978-3-540-30429-6, **2008**, pp. 1437–1472.
[18] U. Heinze, D. Klemm, E. Unger, F. Pieschel, *Starch - Stärke* **2003**, *55*, 55.
[19] L. Passauer, H. Bender, *Carbohydr. Polym.* **2017**, *168*, 356.
[20] N. S. Zubkova, T. A. Kachalina, M. A. Tyuganova, *Fibre Chem.* **1993**, *24*, 450.
[21] Y. Yuan, H. Yang, B. Yu, Y. Shi, W. Wang, L. Song, Y. Hu, Y. Zhang, *Ind. Eng. Chem. Res.* **2016**, *55*, 10813.
[22] W. Patrick Lim, M. Mariatti, W. Chow, K. Mar, *Composites, Part B* **2012**, *43*, 124.
[23] S. Gebke, K. Thümmler, R. Sonnier, S. Tech, A. Wagenführ, S. Fischer, *Molecules* **2020**, *25*, 21.
[24] W. Ji, D. Wang, J. Guo, B. Fei, X. Gu, H. Li, J. Sun, S. Zhang, *Carbohydr. Polym.* **2020**, *233*, 115841.
[25] F. Schäfer, Ph.D. thesis, Technische Universität Darmstadt, Darmstadt, **2023**, http://tuprints.ulb.tu-darmstadt.de/23657/.
[26] G. Chen, Z. Liu, S. Deng, W. Zhao, Q.-J. Chen, *J. Appl. Polym. Sci.* **2024**, e56044.
[27] Y. Lu, P. Zhao, Y. Chen, T. Huang, Y. Liu, D. Ding, G. Zhang, *Carbohydr. Polym.* **2022**, *298*, 120076.
[28] S. Gebke, K. Thümmler, R. Sonnier, S. Tech, A. Wagenführ, S. Fischer, *Molecules* **2020**, *25*, 2.
[29] G. Guerrant, D. Brown, *J. Agric. Food Chem.* **1965**, *13*, 493.
[30] D. R. Lide, *CRC handbook of chemistry and physics*, vol. *85*, CRC Press, **2004**.
[31] A. R. Amell, *J. Am. Chem. Soc.* **1956**, *78*, 6234.
[32] I. Nehls, F. Loth, *Acta Polym.* **1991**, *42*, 233.
[33] M. Khalil, S. Farag, K. M. Mostafa, A. Hebeish, *Starch-Stärke* **1994**, *46*, 312.
[34] M. Khalil, S. Farag, A. Aly, A. Hebeish, *Carbohydr. Polym.* **2002**, *48*, 255.
[35] A. Blennow, A. M. Bay-Smidt, C. E. Olsen, B. L. Møller, *J. Chromatogr. A* **1998**, *829*, 385.
[36] H. Maki, M. Tsujito, T. Yamada, *J. Solution Chem.* **2013**, *42*, 1063.
[37] H. E. Gottlieb, V. Kotlyar, A. Nudelman, *Asian J. Org. Chem.* **1997**, *62*, 7512.
[38] M. J. Tizzotti, M. C. Sweedman, D. Tang, C. Schaefer, R. G. Gilbert, *J. Agric. Food Chem.* **2011**, *59*, 6913.
[39] C. Noè, C. Tonda-Turo, A. Chiappone, M. Sangermano, M. Hakkarainen, *Polymers* **2020**, *12*, 1359.
[40] M. Kolen, W. A. Smith, F. M. Mulder, *ACS omega* **2021**, *6*, 5698.
[41] M. Bhogadia, M. Edgar, K. Hunwin, G. Page, M. Grootveld, *Metabolites* **2023**, *13*, 792.
[42] A. Idström, S. Schantz, J. Sundberg, B. F. Chmelka, P. Gatenholm, L. Nordstierna, *Carbohydr. Polym.* **2016**, *151*, 480.
[43] A. McPherson, J.-l. Jane, *Carbohydr. Polym.* **1999**, *40*, 57.

[44] B. G. Fiss, L. Hatherly, R. S. Stein, T. Friščić, A. Moores, *ACS Sustainable Chem. Eng.* **2019**, *7*, 7951.
[45] M. Kroger, O. Badara, T. Paakkonen, I. Schlapp-Hackl, S. Hietala, E. Kontturi, *Biomacromolecules* **2023**, *24*, 1318.
[46] S. Azeroual, A. Belfkira, H. Wattati, M. Taourirte, R. Jalal, *Starch-Stärke* **2023**, *75*, 2300071.
[47] G. Camino, L. Costa, L. Trossarelli, *Polym. Degrad. Stab.* **1985**, *12*, 203.
[48] Y. Sang, O. Prakash, P. A. Seib, *Carbohydr. Polym.* **2007**, *67*, 201.
[49] R. Kizil, J. Irudayaraj, K. Seetharaman, *J. Agric. Food Chem.* **2002**, *50*, 3912.
[50] S. Cael, J. Koenig, J. Blackwell, *Carbohydr. Res.* **1973**, *29*, 123.
[51] E. Pigorsch, *Starch-Stärke* **2009**, *61*, 129.
[52] A. Abdullah, S. Chalimah, I. Primadona, M. Hanantyo, *IOP Conf. Ser.: Earth Environ. Sci* **2018**, *160*, 012003.
[53] M. Sekkal, V. Dincq, P. Legrand, J. Huvenne, *J. Mol. Struct.* **1995**, *349*, 349.
[54] P. Vasko, J. Blackwell, J. Koenig, *Carbohydr. Res.* **1972**, *23*, 407.
[55] E. Wiercigroch, E. Szafraniec, K. Czamara, M. Z. Pacia, K. Majzner, K. Kochan, A. Kaczor, M. Baranska, K. Malek, *Spectrochim. Acta, Part A* **2017**, *185*, 317.
[56] J. Ni, L. Chen, K. Zhao, Y. Hu, L. Song, *Polym. Adv. Technol.* **2011**, *22*, 1824.
[57] P. D. Vasko, J. Blackwell, J. Koenig, *Carbohydr. Res.* **1971**, *19*, 297.
[58] U. Braun, A. I. Balabanovich, B. Schartel, U. Knoll, J. Artner, M. Ciesielski, M. Döring, R. Perez, J. K. Sandler, V. Altstädt, T. Hoffmann, D. Pospiech, *Polymer* **2006**, *47*, 8495.
[59] A. Battig, J. C. Markwart, F. R. Wurm, B. Schartel, *Polym. Chem.* **2019**, *10*, 4346.
[60] G. Socrates, *Infrared and Raman characteristic group frequencies: tables and charts*, John Wiley & Sons, **2004**.
[61] C. Greenwood, *Advances in Carbohydrate Chemistry*, vol. *22*, Academic Press, **1967**, pp. 483–515. https://www.sciencedirect.com/science/article/pii/S0096533208601575.
[62] L. Passauer, *Carbohydr. Polym.* **2019**, *211*, 69.
[63] A.-A. Nada, S. Mohamed, M. El-Sakhawy, *Polym. Degrad. Stabil.* **2000**, *70*, 347.
[64] R. J. Zaldivar, G. L. Ferrelli, H. I. Kim, *J. Compos. Mater.* **2022**, *56*, 1349.
[65] G. Camino, L. Costa, L. Trossarelli, *Polym. Degrad. Stab.* **1984**, *7*, 221.
[66] M. Lowenthal, R. Khanna, M. Moore, *Spectrochim. Acta A Mol. Biomol. Spectrosc.* **2002**, *58*, 73.
[67] M. A. Sherief, A. A. Hanna, A. S. Abdelmoaty, *Can. J. App. Sci* **2014**, *3*, 94.
[68] G. Camino, L. Costa, L. Trossarelli, *Polym. Degrad. Stab.* **1984**, *6*, 243.
[69] L. Passauer, F. Liebner, K. Fischer, in, *Macromol. Symp.* , vol. *244*, Wiley Online Library, **2006**, pp. 180–193.
[70] S. Duquesne, M. Le Bras, S. Bourbigot, R. Delobel, F. Poutch, G. Camino, B. Eling, C. Lindsay, T. Roels, *J. Fire Sci.* **2000**, *18*, 456.
[71] D. Bryce, C. Greenwood, *Starch-Stärke* **1965**, *17*, 275.
[72] X. Liu, Y. Wang, L. Yu, Z. Tong, L. Chen, H. Liu, X. Li, *Starch-Stärke* **2013**, *65*, 48.
[73] Q.-Q. Ouyang, Z. Hu, S.-D. Li, W.-Y. Quan, L.-L. Wen, Z.-M. Yang, P.-W. Li, *Food Chem.* **2018**, *264*, 277.
[74] D. Bryce, C. Greenwood, *Starch-Stärke* **1963**, *15*, 285.
[75] D. J. Bryce, C. Greenwood, *Starch-Stärke* **1963**, *15*, 359.
[76] J. Zhang, M. W. Nolte, B. H. Shanks, *ACS Sustainable Chem. Eng.* **2014**, *2*, 2820.
[77] K. Kato, *Agric. Biol. Chem.* **1967**, *31*, 657.
[78] Y. Liu, L. Yang, C. Ma, Y. Zhang, *Materials* **2019**, *12*, 5.
[79] X. Zhang, J. Golding, I. Burgar, *Polymer* **2002**, *43*, 5791.
[80] P. Tomasik, S. Wiejak, M. Pałasiński, in *Adv. Carbohydr. Chem. Biochem.* , vol. *47*, Elsevier, **1989**, pp. 279–343.
[81] X. Zhu, Q. He, Y. Hu, R. Huang, N. Shao, Y. Gao, *J. Therm. Anal. Calorim.* **2018**, *132*, 927.
[82] M. Piglowska, B. Kurc, L. Rymaniak, P. Lijewski, P. Fuć, *Polymers* **2020**, *12*, 2.
[83] B. Kaur, I. S. Gur, H. L. Bhatnagar, *Angew. Makromol. Chem.: Appl. Macromol. Chem. Phys.* **1987**, *147*, 157.
[84] S. Rabe, Y. Chuenban, B. Schartel, *Materials* **2017**, *10*, 455.
[85] K. Wu, Y. Hu, L. Song, H. Lu, Z. Wang, *Ind. Eng. Chem. Res.* **2009**, *48*, 3150.
[86] X. Liu, L. Yu, F. Xie, M. Li, L. Chen, X. Li, *Starch - Stärke* **2010**, *62*, 139.
[87] R. K. Jain, K. Lal, H. L. Bhatnagar, *Thermochim. Acta* **1986**, *97*, 99.
[88] B. Schartel, B. Perret, B. Dittrich, M. Ciesielski, J. Krämer, P. Müller, V. Altstädt, L. Zang, M. Döring, *Macromol. Mater. Eng.* **2016**, *301*, 9.
[89] G. Heymer, H. Harnisch, Process for the manufacture of ammonium polyphosphate, **1972**, US Patent 3,645,674.
[90] H. Hahn, H. Heumann, H. Liebing, M. Schweppe, W. Hilt, Process for the manufacture of ammonium polyphosphate, **1978**, US Patent 4,104,362.
[91] Y. Lin, B. Yu, X. Jin, L. Song, Y. Hu, *RSC Adv.* **2016**, *6*, 49633.
[92] G. J. Minkoff, C. F. H. Tipper, *Chemistry of combustion reactions*, Butterworths, **1962**.
[93] Z.-B. Shao, C. Deng, Y. Tan, L. Yu, M.-J. Chen, L. Chen, Y.-Z. Wang, *J. Mater. Chem. A* **2014**, *2*, 13955.
[94] Y. Tan, Z.-B. Shao, L.-X. Yu, J.-W. Long, M. Qi, L. Chen, Y.-Z. Wang, *Polym. Chem.* **2016**, *7*, 3003.
[95] N. Vollmer, R. Ayers, *Int. J. Self Propag. High Temp. Synth.* **2012**, *21*, 189.
[96] S.-S. Chang, *Polymer* **1992**, *33*, 4768.
[97] M. Michel, E. Ferrier, *Constr. Build. Mater.* **2020**, *231*, 117206.

